BRNO UNIVERSITY OF TECHNOLOGY
VYSOKÉ UČENÍ TECHNICKÉ V BRNĚ

FACULTY OF MECHANICAL ENGINEERING
FAKULTA STROJNÍHO INŽENÝRSTVÍ

ENERGY INSTITUTE
ENERGETICKÝ ÚSTAV

DISC FRICTION LOSS IN CENTRIFUGAL PUMPS AND HYDRAULIC TURBINES
DISKOVÉ ZTRÁTY ODSTŘEDIVÝCH ČERPADEL A VODNÍCH TURBÍN

SHORT VERSION OF DOCTORAL THESIS
ZKRÁCENÁ VERZE DIZERTAČNÍ PRÁCE

AUTHOR — Ing. Lucie Zemanová
AUTOR PRÁCE

SUPERVISOR — doc. Ing. Pavel Rudolf, Ph.D.
ŠKOLITEL

BRNO 2022

Keywords

Sidewall gap flow, Disk friction losses, Rotating cavity, Instability, Axial thrust, CFD, Centrifugal pumps, Turbines, Hydraulic machines, Turbomachinery

Proudění v mezidiskových spárách, diskové ztráty, spára mezi rotorem a statorem, axiální síla, CFD, odstředivá čerpadla, turbíny, hydraulické stroje

ISBN (80-214-)
ISSN 1213-4198

Contents

Introduction

Despite the sidewall gaps of hydraulic machines are tiny spaces and the volume of the fluid inside it is orders of magnitude smaller compared to the other dimensions of a pump or a turbine, the character of the flow in their interiors can significantly influence the flow in the machine in general. It consequently impacts its operation, efficiency, and reliability. Moreover, the theoretical description of the flow near rotating disks as well as its numerical simulation is a challenging task.

Disk-shaped cavities filled with fluid are common in applications, such as torque converters of an automatic gearbox, magnetic storage devices, or semiconductor manufacturing processes with rotating wafers in electronics. Nevertheless, the most important industrial application is associated with flow in sidewall gaps in turbomachinery.

With the increasing knowledge in fluid mechanics as well as in turbomachinery, it became evident that the flow in the sidewall gaps is a quite complex problem. Even the solution of the flow in a simple cylindrical cavity is not trivial and involves a wide variety of regimes and structures. Moreover, the geometry of the gaps in hydraulic machines is not as simple as in reported research studies. Furthermore, it is complicated by the presence of throughflow, which is not negligible, since it has certain consequences in various related phenomena. The most important issues that are directly governed by the flow inside the sidewall gaps are disk friction and axial thrust.

Increasing demands on the performance of all devices are undoubtedly connected with understanding the phenomena occurring inside these systems. Description of the underlying physics and prediction of possible conditions may lead to machine design optimization, an increase of performance, cost reduction, better reliability, and in the final consequence, to higher efficiency.

However, the understanding of the flow in sidewall gaps of hydraulic machines is limited, since it is based on the theory and observations obtained for very simplified assumptions. Its applicability in turbomachinery is doubtful. Experiments on rotating cavities, which are by its shape closer to the real pumps or turbines, are missing, there are also unanswered questions about the appropriate approach to numerical modeling.

The thesis aims to bring better insight into the flow in sidewall gaps of centrifugal pumps, study the impact of the flow on phenomena significant for its operation and find a suitable approach to numerical simulations of such types of problems.

CHAPTER 1

Flow inside rotating cavities

1.1 Parameters for the description of flow

In order to characterize the geometry of the rotor-stator cavity and operating conditions, several parameters are defined according to the following equations and Figure 1.1. The regime of the flow can be described by a combination of two nondimensional variables: aspect ratio G and rotational Reynolds number Re. The aspect ratio expresses the influence of the geometry, while the rotational Reynolds number involves the effect of operating conditions.

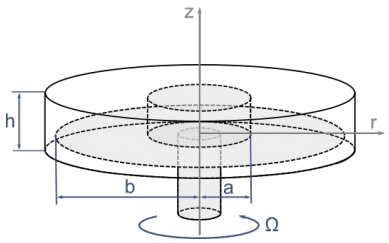

Figure 1.1. Designation of variables for characterization of the flow in sidewall gap

$$G = h/b, \tag{1.1}$$

where h is the width of the gap and b is the outer radius, as is shown in Figure 1.1.

$$Re = \frac{\Omega b^2}{\nu}, \tag{1.2}$$

where b is a typical length scale (in the case of enclosed cavity outer radius), Ω is rotational speed and ν is the kinematic viscosity of the fluid.

1.2 Flow regimes and patterns in rotor-stator cavity

Daily and Nece [1] studied the problem of flow in enclosed cavities experimentally. They proved the existence of four different regimes. The flow can be laminar or turbulent and the boundary layers can be either separated or merged.

The state of the flow is governed by a combination of dimensions of the cavity and the operating conditions given by the nondimensional variables Re and G, which were defined in the first section of this chapter. Four regimes according to Figure 1.2 are then possible:

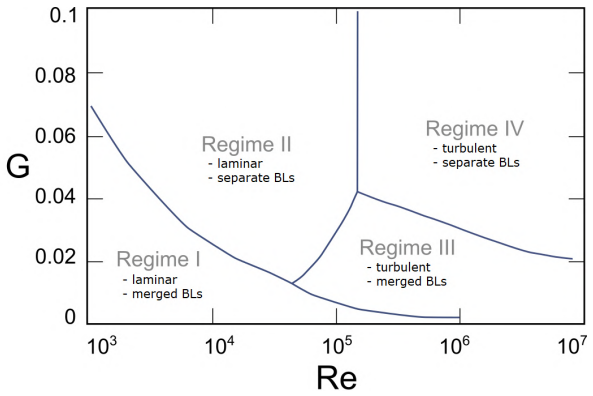

Figure 1.2. Map of regimes [2]

Regimes I and III

Those regimes are often denoted as small clearance cases and can be described as torsional viscous Couette-type of flow. The radial velocity profile is an S-shaped curve with a flow of outward direction along with the rotor and inward flow near the stator. The tangential component of velocity varies linearly across the gap, as shows the following figure. For large aspect ratios of the cavity, these regimes may never exist. For industrial applications, regime III is usually more relevant due to higher Re. The frictional resistance for those regimes decreases with increasing gap width as a consequence of the reduced velocity gradient [3].

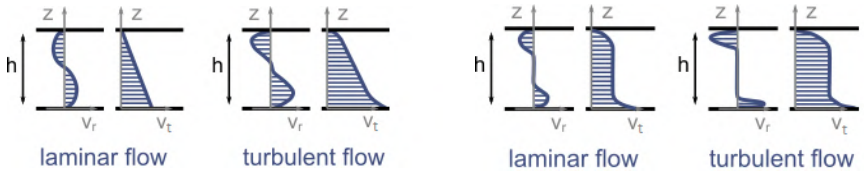

Figure 1.3. Velocity profiles of small clearance (left) and large clearance (right) regimes [4]

Regimes II and IV

The flow is usually referred to as Batchelor type or a large clearance flow. For those regimes, the boundary layers along the rotor and stator are separated by an inviscid rotating core. The boundary layer on the rotor is termed the Ekman layer, while the boundary layer on the stator is the Bödewadt layer. The radial component of the flow at the rotor is positive (outward direction) and is compensated by the inward radial velocity at the stator. The tangential component of velocity in the Ekman layer changes between the speed of the disk and the core speed. The radial velocity component approaches zero in a major part of the domains except for the regions near the confining cylinders as shows Figure 1.3.

Instabilities and transitions, throughflow

A wide variety of unstable structures and transition scenarios among all previously described flow regimes may occur. The stability is principally governed by the boundary layers of the disks. Additionally, the presence of the hub and shroud influences the global stability as well and causes a difference between theoretical results for infinite disks and experiments with real geometry. An occurrence of various structures was observed (spiral or circular rolls, turbulent spots, solitary waves, etc. depending, again, on the geometry and operating conditions. For the complex review and map of identified instabilities see Schouveiler et al. [5].

The effect of the presence of throughflow on the flow patterns inside the rotating cavities was studied due to its relevance to turbomachinery, e.g., in [6–9]. Hide [6] noted that for the laminar regime even a very slight increase in the mass flow rate results in instability. A series of experimental measurements for the turbulent regime [7] revealed that with increasing flow rate, the width of the central flow grows and as a consequence, the depth of the Ekman boundary layer decreases. The effect of the throughflow direction (whether the fluid enters the cavity axially or radially) was also studied. The major difference was described in the size and nature of the flow in the immediate vicinity of the inlet. In the case of the radial inlet, the flow is gradually destabilized by large-scale instabilities occurring as a consequence of Ekman layer onset while increasing Re. Contrarily, the axial inlet forces recirculation and the occurrence of Ekman layer instability and/or vortex breakdown in the central region causing unsteady flow despite the value of Re, under all observed conditions.

1.3 CFD simulation of the flow in rotor-stator cavities

It should be emphasized that modeling the flow between stationary and rotating disks is a quite challenging task for CFD. The flow structures can be very complex, involving laminar, transitional, and turbulent regions at the same time. Moreover, as a consequence of rotation effects, the turbulence is inhomogeneous and anisotropic. Many different approaches to modeling can be found in the literature.

Chew [10] performed a calculation of the rotating cavity flow using the most simple approach: RANS equations and high Reynolds eddy viscosity model k-ε with wall functions approximation. He found out that this model is not able to predict at least the major flow characteristics obtained by measurement. Chew and Vaughan [11] obtained more satisfactory results with low Reynolds mixing-length models, which use the integration of flow equations over the wall sublayer region. Promising results with RSM model achieved Poncet et al. [12] for a rotating cavity with centrifugal and centripetal throughflow. Poncet et al. [13] carried out a study to compare the capabilities of k-ω model introduced by Wilcox [14] and SST k-ω model developed by Menter [15] with k-ε and RSM. It was found out that all tested models failed to predict the thickness of boundary layers. Even though the RANS models provide a reasonable overview of the base flow inside rotating cavities, they are not able to describe the behavior in the boundary layers precisely and even though an unsteady algorithm is applied,

the instabilities are not predicted. For these reasons, studies based on DNS such as [16] or [17] appeared. This approach did not allow to solve complex cases based on real geometry and flow with higher Re, hence it was substituted by a slightly simpler LES. Lo et al. [18], Pasquetti et al. and [19] solved the flow using LES. Comparison of radial and tangential velocity profiles confirmed that the LES model gives results much closer to the experimentally obtained data than the laminar solution or k-ε turbulence model. Unstable structures aligned with the tangential direction can be observed. The overall agreement in velocity components is also good, and the method was found to be applicable for higher Reynolds numbers than DNS.

1.4 Disk friction losses

Disk friction losses appear on a shroud and a hub of an impeller rotating in the fluid. It has a significant impact on the overall efficiency, especially in the case of centrifugal machines with low or moderate specific speeds. According to Gülich [20], at a specific speed, $n_q = 10$, the power losses due to the disk friction reach typically about 50 % of the useful power. This applies also to low specific speed turbines, especially when operating in off-design conditions, as described Trivedi [21]. Thus, there is a need to be able to estimate the disk friction losses during the design phase.

An estimation of the disk friction is based on a simplified case of the plain disk rotating in an enclosed cylindrical casing using the local friction coefficient c_f generated on the surface of a rotating disk. It is determined experimentally, and many different empirical equations derived by fitting the measured data were obtained. A complex explanation of the influence of the established flow regime was published by Daily and Nece [22]. By experimental measurement of friction torque, they quantified the effect of a particular flow regime using a variable called moment coefficient c_m:

$$M = c_m \frac{1}{2} \rho \omega^2 b^5. \tag{1.3}$$

For different Re representing different flow regimes (I-IV) the friction torque M was measured and equations describing the moment coefficient were derived. For particular equations see [22].

Nece and Daily [22], Poullikkas [23] studied also the influence of surface roughness. Daily et al. [24], Owen [25] dealt with the influence of throughflow, Hu et al. revised the influence of throughflow and the flow direction (centripetal [2] vs centrifugal [26] flow). The problem of experimental data correlation was discussed, since the obtained values for the same Re strongly depend on the design and setup of the particular experimental rig, despite the derived equations are based on the same theoretical background. The agreement of previously performed experiments with new measurements was about 10 %. Moreover, there is questionable applicability to real hydraulic machines. Most of the experiments were performed on simple annular geometry with steady operating conditions, which is not always true in turbomachinery. As a result of optimization and years of development, complex shapes of sidewall gaps or features such as labyrinth seals are commonly used in hydraulic machines. Further uncertainty presents the presence of throughflow and requirements for a wide range of operating conditions leading to unsteady flows. About 40 to 70 % higher losses than expected based on the estimations for plain disk in a cylindrical casing were obtained by measurements in volute casings [27].

Gülich [20] investigated the effects determined by real shapes of an impeller, which influence the disk friction. He derived equations considering the true geometry of a pump impeller without simplification. Other authors modified the equations in order to involve operating conditions, which plays the most significant role in real hydraulic machines, which are Reynolds number, axial gap, surface roughness, boundary layer, shape of the stator and sidewall gaps, leakage flow, partload recirculation, exchange of momentum.

1.5 Axial thrust

Axial thrust is a result of unbalanced forces acting on the rotor of the pump in the axial direction. The resulting force is a sum of sub forces caused by the pressure distribution on the shrouds F_{DS} and F_{TS}, the momentum F_I, unbalanced forces F_w on the shaft and the rotor weight, as illustrates Figure 1.4 [28]. As it is given by the flow field in the hydraulic machine, it is closely connected with the flow inside sidewall gaps. Forces caused by uneven pressure distribution on the shrouds are influenced by many various effects, such as type of the pump, type of diffuser, flow rate, design of the impeller, and the pump body [29].

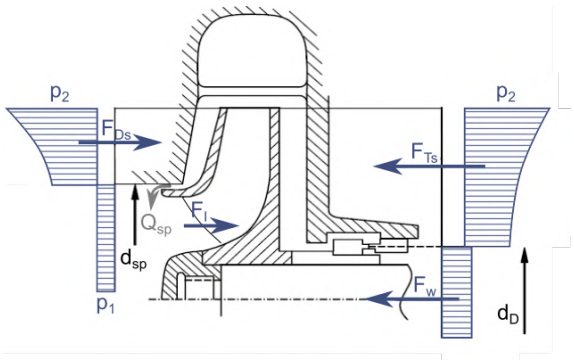

Figure 1.4. Pressure distribution and axial forces acting on an impeller [28]

From the design point of view, it is crucial to consider the axial thrust in the choice of bearings. Many failures due to the axial movement of the rotor are known, leading to complete damage of a machine. the imbalances influence the stability of the operation and the dynamics of the whole system. Periodical loading can cause wearing if the bearings are not chosen properly with respect to axial forces. Since the reliability and service time is determined by this factor, there is a strong need to estimate the value of axial thrust.

There are equations to determine the particular components of axial thrust, however, they were, as in the case of the disk friction, derived considering many simplifying assumptions. Therefore, they provide results, which can be significantly different from measurements. The general assumption is that the liquid in the impeller sidewall gaps has a velocity equal to half of the circumferential speed of the impeller. The next assumption states that the pressure distribution on the impeller outer diameter is uniform. This results in a parabolic distribution of the pressure in the impeller sidewall gaps. For details see e.g. [29–31]. All published studies agree that there are two main factors influencing the resulting axial thrust: character of flow in the impeller sidewall gap and pressure distribution at impeller outlet.

CHAPTER 2

Objectives

The purpose of the thesis is to extend the current state of the art in the flow inside sidewall gaps of hydraulic machines by obtaining a better understanding of its consequences on the phenomena of disk friction losses and axial thrust.

Experimental studies are limited to the cases with simplified geometry (a plain disk rotating in a cylindrical casing). Such an approach gives only a limited idea of the flow and is not capable of capturing undoubtedly significant effects caused by blades of the impeller and complex shapes of real geometry in general. Despite we are aware of the existence of various unstable flow structures and the conditions under which they occur, the applicability of those findings in real turbomachinery problems is uncertain.

The impact of the presence of unstable flow structures in sidewall gaps on disk friction losses and axial thrust is also unclear. The presence of a real impeller with a certain number of blades can possibly disturb the flow field in the backside wall gap and makes the applicability of previous findings even more doubtful.

The aim of the thesis is to describe the possible regimes and flow structures appearing in the sidewall gaps of the real shaped impeller and to put it into the context of disk friction losses and axial thrust.

Particular objectives of the doctoral thesis:

- Methodology of CFD for flow in rotor-stator gaps capable of capturing all possible flow regimes
- Design of an experimental apparatus with inner geometry close to the real pump, which enables simultaneous observation of flow regimes and measurements of disk friction losses and axial thrust
- Experimental measurements supported by CFD simulations
- Summary of new findings and conclusions applicable in turbomachinery

CHAPTER 3
Experimental apparatus

3.1 Requirements

In order to study flow regimes in the back-sidewall gap, an experimental apparatus will be built. It should enable:

- To study experimentally the flow in the back-sidewall gap of a real hydraulic machine with appropriate, not over-simplified, geometry of the gap
- To use a real impeller
- Visualisation of the flow in the back-sidewall gap using an optical method, such as particle image velocimetry (PIV) or laser doppler anemometry (LDA)
- Achieving various flow regimes and possible transitions in the gap
- Measurement of disk friction and axial thrust
- Comparison with CFD results
- Modifications of the impeller, e.g. back vanes, in order to study the influence on axial thrust (for future studies)

3.2 Design of experimental apparatus

The experimental apparatus was designed in a way, that it can use the impeller, which was available in our laboratory from previous research. It was originally taken from low specific speed pump Beta 14, for more details see [32]. Using an impeller from a low specific speed pump enables us to emphasize the effect of disk friction, which plays a very important role in this type of pump. Moreover, the flat hub allows modifications, such as experiments with back vanes and research of the features for mitigation of axial thrust. The impeller was modified by covering the hub with a 1.5 mm thin plate in order to achieve a design, which is more common and which allows to equip back vanes for axial thrust reduction.

The main purpose of the apparatus is an experimental investigation of the flow in the back-sidewall gap, behind the impeller. In order to achieve various flow regimes, the apparatus should enable the regulation of rotational speed and the height of the back-sidewall gap. The design assumes the existence of different regimes and transitions in a similar range of Re and G

to previously obtained map [1]. A possible shift towards lower Re is presumed, so relatively wide range was chosen to cover it, as shows Figure 3.1. Since the impeller diameter $D = 320$ mm is given by the existing component, the maximum gap width $h = 19.2$ mm and rotational speed $\Omega = 320$ rpm for experimental visualisation was determined, as summarizes Figure 3.1.

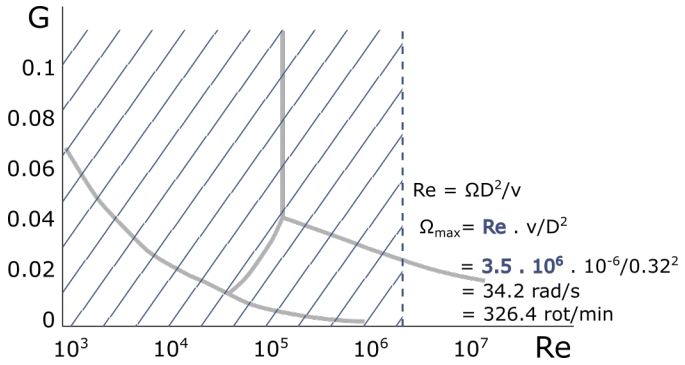

Figure 3.1. Determination of design parameters for the apparatus

The principle of the change of the back-sidewall gap width h illustrates Figure 3.2 left. The desired position of the back cover, which defines the gap, is achieved by inserting a spacing ring of particular width g.

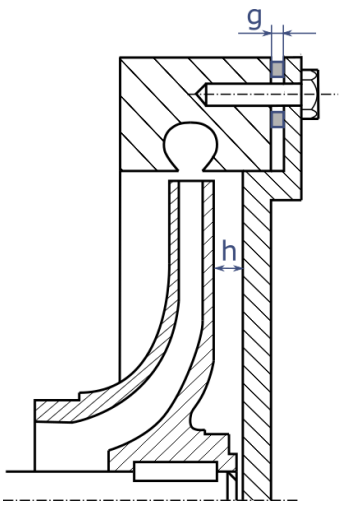

g (mm)	h (mm)
0	3.46
6.3	9.76
1.5 + 8	12.96
6.3 + 1.5 + 8	19.26
1.5	4.96
6.3 + 8	17.76

Figure 3.2. Principle of the change of the gap width h by inserting spacing ring (left), different spacer widths and achieved back-sidewall clearances (right)

To set wider h, various spacers can be combined together. With a reasonable choice of spacers dimensions, there is no need to manufacture a special spacing ring for each measured gap width h, but reach it by placing 2 spacers on top of each other. The first spacer was machined, which allowed any option of the width g. A clever choice of the dimension enables to use a cheaper manufacturing method for the rest of the spacers, which were cut by water jet from sheet metal semi-finished products. The final choice of the spacer widths g with relevant achieved back-sidewall gap dimensions h is summarized in Figure 3.2 right.

In order to obtain an insight into the flow field in the back-sidewall gap, optical access to the fluid domain of the back-sidewall gap is required, therefore the boundary structures must be constructed from a transparent material (typically glass or Perspex/Plexiglass). 2D PIV for visualization of the single planar section is intended to be employed, which raises a need of a possibility to place the camera outside of the testing rig, perpendicularly to the intended plane of the laser light sheet. The access of laser beam for LDA is designed to be from the front of the cylindrical transparent back part.

LDA

Laser Doppler Anemometry (LDA) was used for the experimental measurement of radial and tangential components of velocity across the back-sidewall gap. LDA equipment was borrowed from the Institute of Water Structures, Faculty of Civil Engineering. FlowExplorer DPSS 300 2D kit for measurement of two velocity vector components was used. It consists of two solid-state lasers with power up to 300 mW, emitting at wavelengths 532 nm and 561 nm, and of a front converging lens with a focal length of 109 mm. The obtained signal was processed by a two-channel BSA F600 2D processor and BSA Flow Software v.6.60. (Dantec). The overall view of the apparatus shows Figure 3.3.

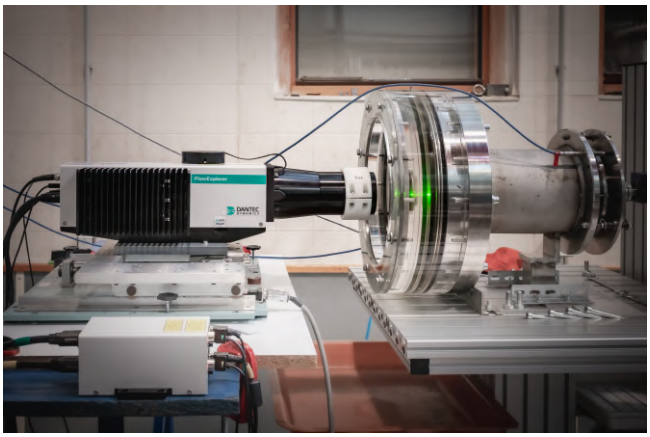

Figure 3.3. LDA setup

The backplate of the impeller was painted in black color to minimize the laser beam reflection and enable the measurement in close proximity of the wall in order to capture the velocity gradient in the boundary layer. It was possible to achieve 14 points across the clearance width starting from the plexiglass cover, aiming perpendicularly to the impeller surface. The radial and tangential velocity components were measured simultaneously. Each measured sequence contains between 5000 and 20 000 samples gathered in 30-second intervals.

Measurement of axial thrust

One of the intended features of the experimental apparatus is a possibility to determine the axial thrust. Its principle is outlined in Figure 3.4. The testing rig consists of parts that

are stationary (mainly the outer cover, indicated in grey) and the parts with allowed axial displacement under the loading (the impeller, the shaft, and tied-up components, indicated in red). The movement is axially guided using ball bushing allowing the translation and rotation provided with minimal friction. It has to be pointed out, that the friction will inevitably take place in such type of connection, however, compared to other methods, such as sliding bearings, it is significantly lower.

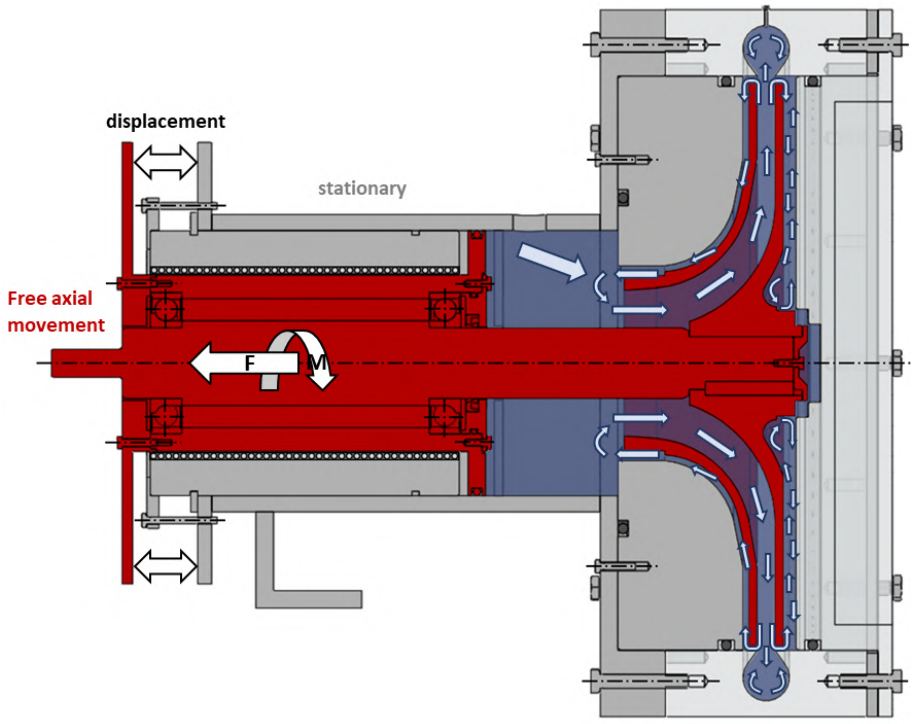

Figure 3.4. Principle of axial thrust measurement

As the fluid flows and creates pressure acting on the impeller, the axially free part of the assembly moves guided by the ball bushing. As a consequence, the distance between marked flanges can be measured. Our laboratory is equipped with sensors of vibrations SCHENCK IN - 085 for the purposes of very precise displacements measurement based on the eddy-current principle. The output voltage of the sensor is proportional to the distance between the probe tip and the measuring surface, within the displacement measuring range of 1.5 mm. The sensors are designed for the measurement of vibrations which are in orders of micrometers, whereas the displacement caused by axial thrust is expected to be orders of magnitude larger. Therefore, the assembly needed to be equipped with added stiffness, which ensures smaller amplitudes of the axial movement. This was provided by 3 sets of pre-loaded springs placed around the flange on threaded rods.

In order to obtain the response of the electric signal to the loading, a calibration had to be performed. The movable part of the apparatus was loaded by calibrated weights, while it was connected to the dynamometer by bellows coupling to ensure that its stiffness is also accounted for. The loading was carried out using a pulley to provide axial direction. The weight corresponding to desired measuring axial thrust range led to the loading up to 7 kg.

The data of the voltage by increasing the weight were obtained, a linear interpolation was performed and the equation describing the dependency of the weight and the corresponding change of the output voltage was derived.

Measurement of disk friction

The experimental apparatus is connected to dynamometer Amtek AMDYN 20, which allows measuring and control of rotational speed. It consists of a driving machine whose output shaft is connected to a strain gauge shaft equipped with coupling for the measurement of torque. The output shaft with a free cylindrical end serves for the connection of a measured machine. Its 10 kW asynchronous servomotor AMK DW 10-20-4-IOW-5000-B5 is driven by a frequency converter allowing to adjust the speed of rotation (0–6000) rpm. The measuring shaft HBM T21W enables measurements in the range of (0–20) Nm with 0.2% accuracy.

The torque is transmitted from the dynamometer output shaft to the driven shaft of the apparatus by flexible bellows coupling STS WK 3-100-48. Its purpose is beside the torque transmission to allow axial displacement of the axially free parts of the testing assembly and therefore the measurement of the axial thrust as was described in the previous section. The stiffness in the axial direction is an order of magnitude smaller than the stiffness of the spring and therefore does not significantly influence the measured displacement and so axial thrust. For precise determination of the torque, the frictional torque of the shaft is subtracted. Therefore, the first step is to measure the torque when the impeller is rotating at different rotational speeds in the air. Measured values in the water are subsequently lowered by corresponding torque obtained in the air.

Experiments with throughflow

To study the effect of the presence of the throughflow in the back-sidewall gap, the apparatus is slightly modified and connected to the tank, as documents Figure 3.5 left. The inlet to the apparatus was manufactured with pipe thread to enable easy connection of a pipe. In order to save resources, the experiments with closed cavity were performed first, then a hole was drilled to the to part of plexiglass volute. The cross sectional area of the inlet is the same as the outlet and therefore the same pipe size can be used for the entire test circuit. The tank is not pressurized, there is a free surface and it is opened to the atmosphere. The pipe leading out of the tank is equipped with valve for the control of the flow rate. It is followed by an magnetic-induction flowmeter IMQI99-SN, DN10/PN40 for its monitoring. There is one absolute pressure probe at the inlet to the apparatus and the second is located at the outlet. The fluid is then led back to the tank. There is also a connection to a water supply, which besides water filling serves also for deaeration of the system. The layout of the test circuit with the locations of the sensors is shown in Figure 3.5 right. The signals from the both pressure sensors as well as from the flowmeter are collected by a measuring cards and processed using LabVieW software interface.

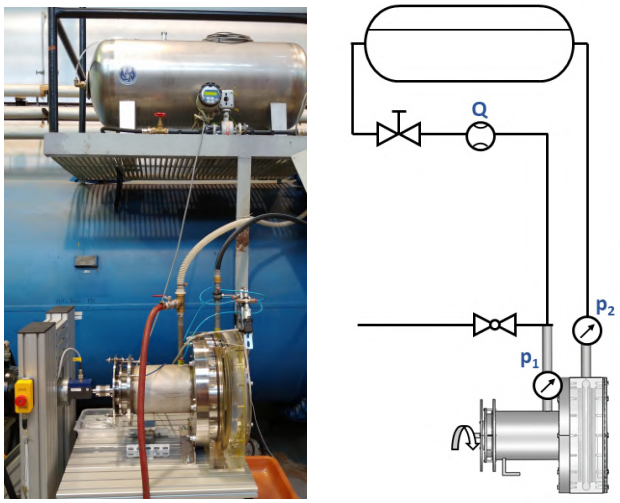

Figure 3.5. Experimental circuit for measurement with throughflow and its scheme

3.3 Design of experiment

For the purposes of this thesis, the scope of the research needs to be narrowed, and limited but meaningful number of geometrical configurations to study has to be chosen. In order to achieve different flow regimes, four heights of the clearance were chosen according to Table 3.1.

h_1	3.46 mm
h_2	9.76 mm
h_3	12.96 mm
h_4	19.26 mm

Table 3.1. Heights of the back-sidewall gap

For financial situation, it was not possible to realize PIV, nor more than one set of measurements using laser methods. Considering this, the set of measurements will be used for verification of the CFD model and subsequent parts of the study will be based on the numerical computations. For the mentioned measurement, the medium width of the back-sidewall gap clearance $h_2 = 9.76$ mm was chosen. The measurement with the narrower gap would be problematic because of extreme demands on laser and positioning system precision, while the width h_2 provides better practicability and the transition between regimes should be observable as well. Moreover, it corresponds the commonly used range of G in turbomachinery according to [28, 33]. The measurements were carried out on a closed configuration (without throughflow). Covered range of rotational speeds was $\Omega = (10, 20, 40, 80, 160, 320)$ rpm.

As the next step, it is necessary to choose positions for which LDA measurement of velocity components will be performed. Limits are given by the laser light refraction on the plexiglass edges close to the outer impeller diameter and the shaft. The available LDA equipment restricts the endpoints locations to maximal radius $R = 134$ mm and minimal radius $R = 40$ mm.

Three locations evenly distributed over the back-sidewall gap were added to cover the flow field in most of the back-sidewall gap domain, as documents Figure 3.6. Radial and tangential components of velocity were captured at 30-second intervals in 14 locations across the gap.

R_1	134 mm
R_2	115 mm
R_3	96 mm
R_4	68 mm
R_5	40 mm

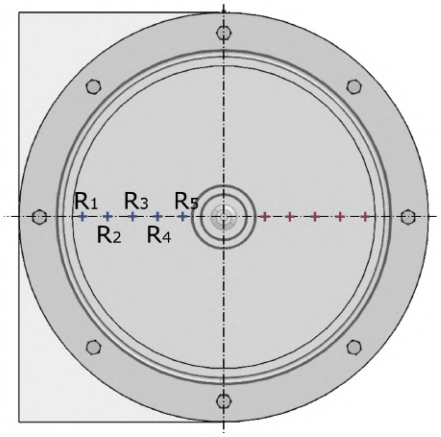

n (rpm)	left	right
10	✓	✓
20	✓	✗
40	✓	✓
80	✓	✓
160	✓	✗
320	✓	✓

Figure 3.6. Radial locations for LDA and overview of measured rotational speeds

Since there was a suspicion of possible asymmetry of the flow field, although there was no obvious reason for that, it was decided to do the measurement on both, left and right, sides of the back-sidewall gap in order to confirm or disprove it. As those measurements were relatively time-consuming, the number of measured rotational speeds on the right-hand side was slightly reduced. The complete overview of accomplished LDA measurement is given by Figure 3.6 right.

Torque was measured for all four gap heights ($h_1 - h_4$) in such a way, that rotational speed was increasing from 0 to 320 rpm by 20 rpm. Afterward, the values obtained for corresponding speed in the air were subtracted.

Axial thrust was measured at the same time as the torque, therefore for all gap heights, the rotational speed was increasing from 0 to 320 rpm by 20 rpm.

In order to study the influence of the presence of the thoughflow in the system and not to over-complicate it by another parameters, the back-sidewall gap of the height h_2 was chosen. From the nature of the machine (centrifugal pump), the flow rate is changing with the rotational speed. Therefore, it is not possible to maintain a constant flow-rate for different rotational speeds without using an external pump, as was performed in previous studies of the throughflow with simple cylindrical cavities. The aim of the research is to study the flow in the back-sidewall gaps of real hydraulic machines, therefore it was decided to keep the experiments as close to the real operating conditions as possible. Hence, the flow rate varies over the measured range. The experiments with the throughflow are performed the following way: The maximum considered rotational speed (320 rpm) is set. A desired flow rate is established by the opening/closing the control valve. Its value can be viewed on the flowmeter next to the valve. This value is referred to as the flow rate Q for given set of measurements. To asses the effect of the flow rate to the axial thrust and disk friction, five sets of measurements with different flow rates were performed.

CHAPTER 4
Numerical simulation

4.1 Geometry and mesh

The fluid domain was divided into 5 subdomains (entrance part, impeller, volute, back-sidewall gap, front-sidewall gap). They were connected together by non-conformal interfaces (I–V), as is outlined in Figure 4.1 left. The fluid flows from the entrance part (1) through the interface I to the impeller (2). Interface I separates the stationary fluid zone (1) and rotating fluid zone of the impeller (2). The fluid leaves the impeller zone through one of three interfaces (II, III, or IV) and enters either the volute (3) or one of the sidewall gaps (4,5). The portion of the fluid flowing through the front-sidewall gap returns through interface V to the entrance subdomain and recirculates. The back-sidewall gap subdomain varied with changing of the gap width ($h_1 - h_3$). Due to the very long time required for the simulations, only 3 gap widths were considered, the primary h_2, for which LDA measurements exists and then narrower h_1 and wider h_3. For the calculation with throughflow, the subdomains of entrance and volute slightly differ, since they contain parts for boundary conditions inlet and outlet, whereas, for a closed cavity, there is no need to include it which reduces the demands on the mesh size. The different subdomains for a cavity with throughflow are shown in Figure 4.1 right.

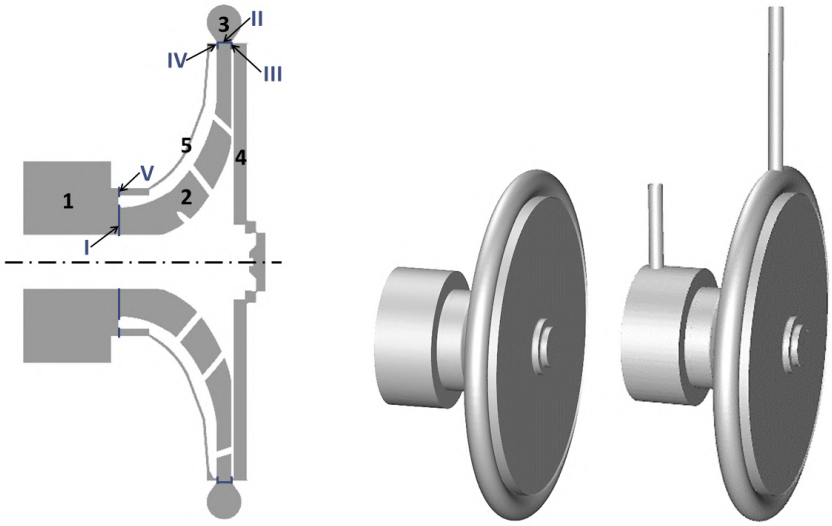

Figure 4.1. Fluid domain overview and its division into 5 parts

4.2 Boundary conditions

No-slip boundary condition is applied on walls. Rotating walls and domains belonging to the impeller are marked by red color, whilst stationary are black. Rotating and stationary zones are coupled by interfaces, whereby the interface between impeller and back-side wall gap treats the transition from RANS to LES turbulence model. According to the FLUENT recommendation and based on previous experience, fluctuating velocity algorithm was set to Vortex Method with a number of generated vortices corresponding to N/4, where N is a number of cells on the interface. For the cases with throughflow, mass flow inlet and pressure outlet is added to the original domain. The lengths of added parts are $5D$ fore the inlet and dimension corresponding to the pressure probe placement for experimental measurement fore the outlet. The values of rotational speed, mass flow rate, and pressure at the outlet for particular cases correspond to experimental measurements. A Water-liquid model from the ANSYS library considering incompressible fluid was used.

4.3 Solver settings

The Embedded LES approach was applied. The main focus was on the flow in the back-sidewall gap, which was treated with LES, whereas the SST k-ω turbulence model was applied to the rest of the domain. WALE subgrid-scale model with Bounded Central Differencing momentum spatial discretization scheme, which is recommended for embedded LES approach, was used. For pressure-velocity coupling, the SIMPLE scheme was used with the first orders of accuracy for advection terms in all transport equations. After achieving convergence on first orders it was switched to the second orders. The time step settings for RANS modeling followed the common practice for CFD in turbomachinery, where for given rotational speed, 2° rotation corresponds to Δt. After achieving convergence and turning on LES in the back-sidewall gap domain, Δt was lowered in an order to fulfill the CFL condition and obtain convergence for embedded LES. By testing, it was found out, that the hybrid initialization works better than the standard one and leads to quicker convergence of subsequent steady-state cases. After 1000 iterations in a steady regime the analysis can be switched to transient with a moving reference frame (MRF). It does not take more than 500 timesteps with 5 inner iterations to converge. Afterward, it is possible to switch to second orders of accuracy. Again, the convergence is achieved relatively quickly, less than 250 timesteps were always sufficient. Next, mesh motion was applied with the number of timesteps corresponding to 2 impeller revolutions for each rotational speed. It turned out to be enough to stabilize the simulation before switching the LES zone on. Enabling LES in the backside-wall domain requires lowering the time step. A few revolutions are computed while observing velocity components in a monitor point until a periodic pattern governed by the passage of blades is developed. Finally, the collection of transient statistics for evaluation and comparison with the experiment is set. The whole sequence is automated by the FLUENT journal file.

CHAPTER 5

Results

The CFD model in general fits very well with LDA measured data in the whole range of rotational speeds. Good agreement is obtained in the central part of the domain in both, the radial and the tangential velocity profiles almost for all radial locations except for $R = 40$ mm. The only discrepancy between numerical and experimental data can be observed in near-wall regions. The reason is limited positioning accuracy of the LDA system, which was not capable of approaching the disks to reach boundary layers reliably, as illustrates following figure. Another sign of a good CFD solution of the velocity gradients in near-wall regions is

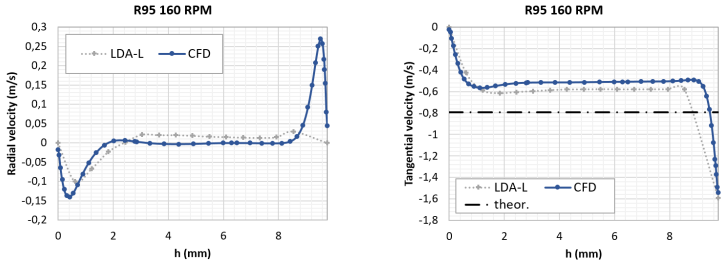

Figure 5.1. Radial velocity profiles comparison

values of frictional torque. The numerical simulation matches the experimental measurement quite well.

Experimental and numerical data agree well for the lower rotational speeds (i.e. 200 rpm). This is likely a result of the choice of the springs, which were primarily designed for the measurement of low forces. For higher forces, and thus, higher displacements, their characteristic may become nonlinear leading to the discrepancy. The chosen springs were the trade-off to do not have to change them during the measurements. It would mean another calibration and considerably complicate the whole process. Nevertheless, measurement with stiffer springs in the range of higher rotational speeds is a good point for future investigation.

5.1 Disk friction

In order to determine torque without influences of friction on the shaft, measurements without water were performed as a first step. Two sets of measurements for various rotational speeds were done and an average value was further used for the subtraction. Unfortunately, data from measurement of h_3 were corrupted and thus are not displayed. Processed data without mechanical friction are then shown in Figure 5.2. The resulting torque increases with increasing rotational speed. There is no sign of changing regimes from III to IV, such as an abrupt change

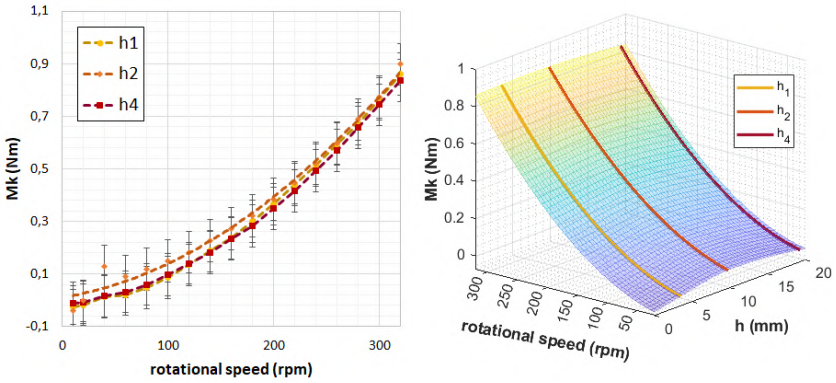

Figure 5.2. Torque depending on rotational speed and gap width

of the trend, which corresponds to the findings presented in [2, 26]. If the dependence on the gap width is considered, it can be seen, that no significant differences were found between the configurations. The friction first decreases with increasing h and later the trend changes and with further increase of h, the torque rises, however, the difference is insignificant and barely recognizable. The finer resolution would be helpful for a better description, especially considering the missing data for h_3.

5.2 Axial thrust

Axial thrust increases with increasing rotational speed approximately quadratically as shows Figure 5.3 left. Its increase is steeper in comparison with the trend for the torque. There is no noticeable change of regime either. No changes of direction were observed, the values which go under 0 for low rotational speeds are within the measurement error.

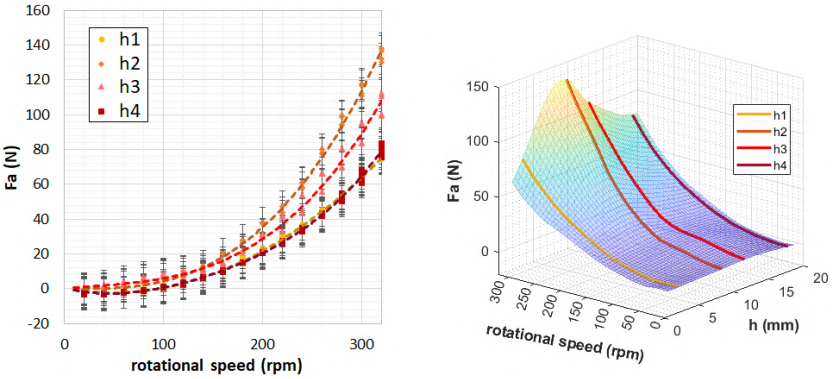

Figure 5.3. Measured axial thrust depending on rotational speed and gap width

The dependence of axial thrust on the back-sidewall gap width is opposite to the torque trend. As illustrates Figure 5.3 right, with increasing h the measured axial thrust tends to increase up to a certain value. Further increase of h results in the decrease of axial thrust on the whole range of rotational speeds. For a more precise description of this phenomenon, measurements with finer resolution (more measured h) would be also here necessary.

5.3 Effect of throughflow

The effect of the presence of the throughflow on the measured torque is negligible. As can be seen in Figure 5.4 the torque does not change with the change of the flow rate, moreover, it stays the same even when the valve is closed (without the throughflow).

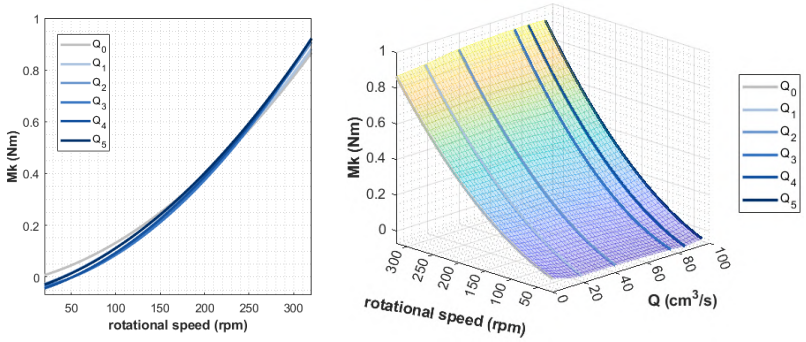

Figure 5.4. Effect of throughflow on torque

On the other hand, the throughflow plays important role in the resulting axial thrust. Its presence and rate change the trend of emerging axial force dramatically, as shows Figure 5.5.

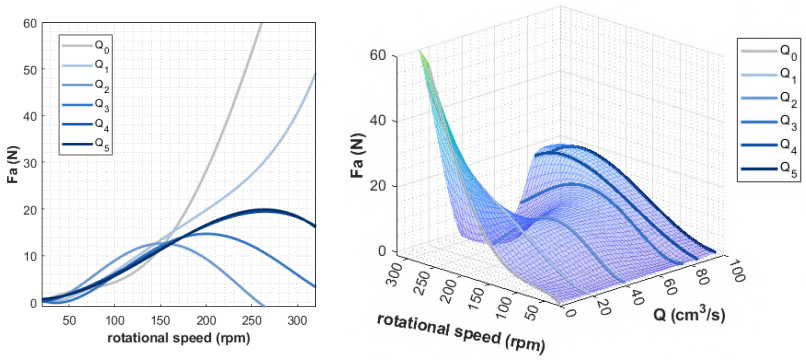

Figure 5.5. Effect of throughflow on axial thrust

It can be seen that for higher imposed flow rates the axial thrust gradually grows with rotational speed first, after achieving its maximum (around 260 rpm) it in the studied range decreases. For lower flow rates the increase is more rapid and the first local maximum is shifted towards lower rotational speeds. The force is almost constant in the range (150 – 250) rpm and afterward, quadratic increase with increasing rotational speed can be observed. The lower the flow rate, the closer is the curve to the one with parabolic shape for zero throughflow (the grey curve in Figure 5.5).

5.4 Flow field in back-sidewall gap

The flow field of the back-sidewall gap domain is quite complex and differs from the flow in a simple rotating cavity, which has been described in previous studies. Even for the higher

rotational Reynolds number, where fully developed regime IV was expected, volume rendering of velocity magnitude with suitable scale reveals the presence of vortical structures in the whole domain, as can be seen in Figure 5.6. It shows the 3D rendering of velocity magnitude across the domain, which has no featureless, monotonous distribution at all. The visualized structures were not recognizable in velocity profiles, since both the experimental and the CFD results were obtained by averaging over time to be able to compare them, therefore those effects were suppressed.

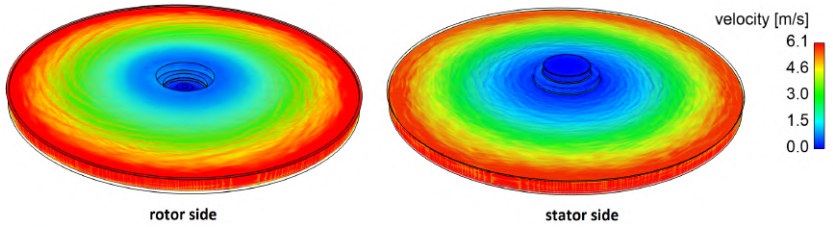

Figure 5.6. Structures in the back-sidewall gap flow field

Nevertheless, the structures are not localized only in near-wall regions, as demonstrates cross-sectional visualization of vorticity in Figure 5.7 and it is also visible in Q-criterion.

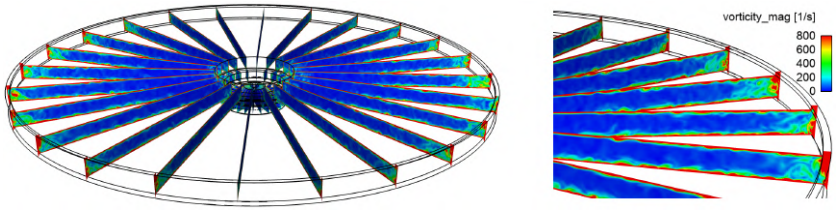

Figure 5.7. Vorticity in gap cross-section

Since the nature of the structures is periodical, it is very likely linked to the rotation of the impeller and the passing of the blades through a particular location. The character evolving with the motion of the blades results in the existence of the angular positions, where the flow enters the domain of the back-sidewall cavity and oppositely, where the fluid returns to the volute part. The changes of fluid direction from and out of the back-sidewall cavity are the link between the spiral structures observable on the rotor side whether in the velocity field, vorticity, or wall shear stress, as shows Figure 5.8. The number of the spiral arms is independent of the rotational speed, if it occurs, 15 separate vortices are always formed. The spirals rotate with the impeller, and 3 of them can be traced in each of the blade channels.

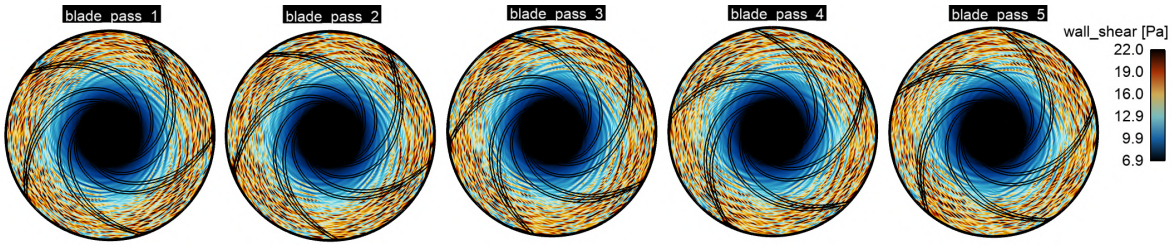

Figure 5.8. Wall shear stress on the rotor side

The evolution of the flow inside the back-sidewall gap with the change of rotational speed of the impeller in the overall picture show Figure 5.9. On the rotor is obvious that with increasing speed, the smooth flow becomes disturbed by the onset of the spiral structures. On the other hand, the stator side is covered with disordered vortices for almost the whole studied range. They disappear for very low rotational speeds (under 10 rpm), but it can be observed as well, that they get gradually weaker when the rotational speed increases over 160 rpm. Visualisation of the flow field in the whole domain reveals that between 20 rpm and 10 rpm the strong vortex at the inlet to the back-sidewall gap disappears and therefore does not influence the flow formation in the whole gap anymore. With the further decrease of the rotational speed to 5 rpm the flow field with uniform character, where the velocity magnitude grows in the axial direction from the stator to the impeller, is developed.

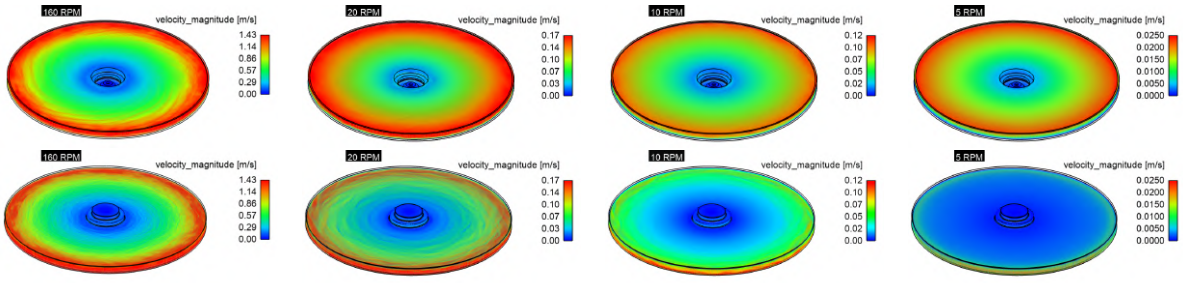

Figure 5.9. Structures near rotor (top) and stator (bottom) for different rotational speeds

The evolution of the flow was studied in detail by means of velocity profiles, similarly to the experimental data processing. For 5 radial positions and each rotational speed the radial and the tangential velocity profiles were plotted, as suggests Figure 5.10.

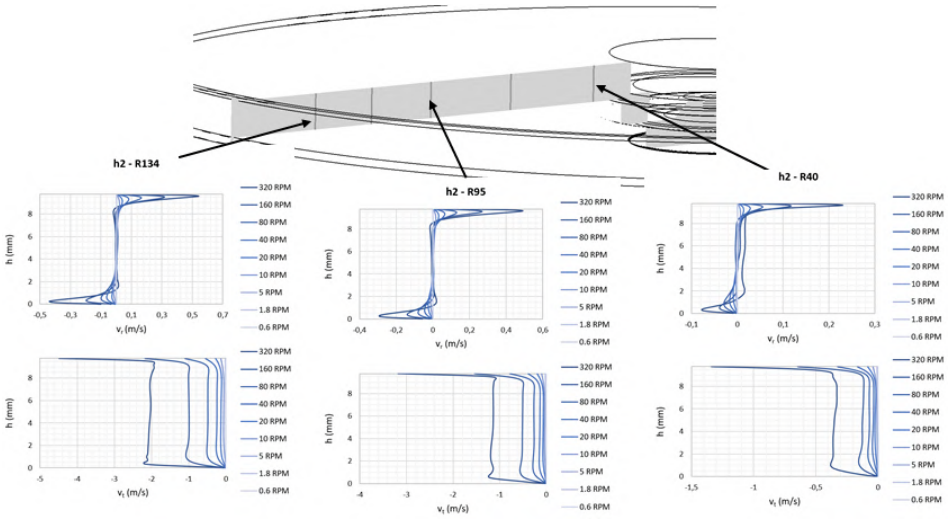

Figure 5.10. Velocity profiles across the back-sidewall gap for different rotational speed

The most of the profiles indicates turbulent flow with separated boundary layers (regime IV) for this gap width (h_2). In fact, any of the radial positions is occupied by this regime when the rotational speed exceed 40 rpm. A typical transition can be observed for rotational speed

under 20 rpm. In the radial velocity profile for 40 and 20 rpm is a clearly distinguishable central vertical region with zero velocity between the gradients belonging to the boundary layers. The analogical shape distinguishing regime IV can be observed in the tangential velocity profile. For 10 rpm the core radial velocity inclines and intervenes both boundary layers, which is the typical evidence of regime III. Below 5 rpm the radial velocity profile becomes S-shaped, which is characteristic of laminar flow with merged boundary layers (regime I). It can be identified also from the change of the tangential velocity profile from curved to straight.

Not every of the possible four flow regimes can develop for a particular combination of gap width, rotational speed, and radial position. Regime II was not detected for any point of the map. The map of regimes obtained experimentally was extended using the CFD data including more rotational speeds and gap widths. More regimes and transitions were identified for such operating conditions which were not reachable experimentally.

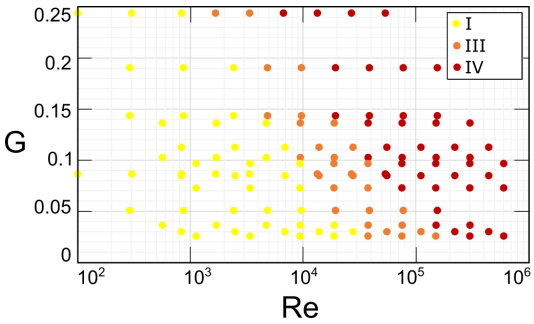

Figure 5.11. Map of regimes obtained from CFD results

Effect of back-sidewall gap width

For the narrower gap h_1, the vortices occur earlier on the rotor side earlier than for the gap h_2, and for h_3 its presence is detected even later. The difference is not only in the speed of the onset of the instability but also in its character. A huge amount of fine spirals is emerging in the narrow gap, stronger spirals can be observed in the middle width and only a few ring-shaped waves propagate in the wide gap. As the rotational speed increases, all of them tend to converge towards the spiral shape of the instabilities described earlier.

The narrower the gap, the less space for the development of variability of the vortical structures. The Q-criterion was not able to detect nearly any vortices in the back-sidewall gap h_1 even for 320 rpm. The narrow gap does not give much space at the inlet to develop the rotating flow and spread the instability, rather mitigates its propagation. The evenly distributed velocity magnitude across the gap radius can be seen up to 40 rpm, whereas for wider gaps h_2 and h_3 the inlet turbulence corrupts the laminar profile already at 10 rpm.

The wider the back-sidewall gap, the more space for the development of diverse patterns of the vortices. For h_2 is the whole gap width filled with vortical structures extending from rotor to stator and those sides interact and influence each other through the flow. On the other hand, in the wider gap h_3 there are structures near the stator, which evolves nearly separately from what is happening on the rotor side. Almost horizontal flow direction appears along the rotor and wavy curved trajectories prevail on the stator without much intervention into each

other. For higher rotational speeds the influence of each side propagates towards the other, however, the separate character is still apparent. Also, the diffusion in the radial direction (to the center of the cavity) is limited in the case of the wider gap h_3, which can be indicated by lower overall velocity magnitude in the central region compared to the gap h_2.

Considering the impact of the gap width on disk friction, no significant differences can be identified. The wall shear stress rises with increasing rotational speed, however, the character of its increase, regions of its maximums are the same for both, the rotor and the stator side, regardless of the gap width. It is in agreement with experimental data, that do not show any difference in the measured torque for different gap configurations.

Flow field in back-sidewall gap with throughflow

Since the intention of the research was to study the flow related to real operating conditions of the pump, it implies low flow rates for the low rotational speed. Although for the CFD simulations the case with a fully opened control valve was chosen, therefore the highest achievable values without using an external pump, it was not sufficient to influence the flow field in the whole pump significantly. The changes in the flow in the back-sidewall gap compared to the same gap configuration without the throughflow were almost indistinguishable up to 80 rpm. No significant differences can be seen neither on vorticity nor on the q-criterion. It can be also noted, that no asymmetry caused by the presence of the outflow is visible.

The first notable influence of the flow field can be seen as the rotational speed increases from 40 rpm to 80 rpm. The stator region is occupied by the instabilities equally, however, spiral vortices on the rotor appear earlier when the throughflow is present. For the closed cavity, no indications of instability can be seen for 80 rpm, while for the case with throughflow the spiral structures are clear. Its earlier onset is possible to identify by the contours of shear stress, nevertheless, the area of the higher shear is almost the same for both cases and thus the different characters do not manifest themselves as a change in the torque.

The comparison of velocity profiles for the case with and without throughflow confirmed the earlier transition to turbulent regime. For low rotational speeds the profiles are almost identical, whereas for 20 rpm it shows that for the case without throughflow the profile still has obviously merged boundary layers in the contraty to the case with throughflow, where the constant core velocity and separated boundary layers can be distinguished.

The only parameter among the observed, that is significantly affected by the presence of throughflow, is the axial thrust. It is given by completely different pressure ratios inside the whole system after connecting it to the test circuit. The pressure acting on the hub and the shroud of the impeller is very different compared to the case of the closed cavity. The pressure distribution on the shroud (front-sidewall gap) is qualitatively similar for both cases and all analyzed rotational speeds, however, its value is an order of magnitude higher with throughflow. Though, the resulting axial thrust is given by the pressure in both front- and back-sidewall gaps. The evolution of the pressure distribution on the hub (i.e. in the back-sidewall gap) is not so straightforward. It evolves with the rotational speed, there is an observable qualitative difference between the closed cavity and the case with the throughflow, moreover, the disparity varies over rotational speed. It results in lower, but more complicated character of resulting axial thrust as was discovered by the measurements.

Conclusion

The objective of the thesis was to investigate the flow inside back-sidewall gaps of the hydraulic machines under various conditions and study its impact on associated phenomena (disk friction and axial thrust). The topic has been covered both, experimentally and by CFD.

It was found out that the simplified theory derived for the rotating disk in a cylindrical cavity and the map of its flow regimes obtained before is not applicable for real machines. The flow field is strongly influenced by the presence of an impeller with a certain number of blades, which governs the flow in the back-sidewall gap. Periodical phenomena linked to the positions of the blades were detected and the rotation of the impeller is a crucial for the development of the flow in the back-sidewall cavity.

The factor that significantly influences the character of the flow is the width of the back-sidewall gap. The wider the gap, the more space for the evolution of various vortices and the greater variability of emerging structures. The narrower gap, the formation of vortices is suppressed at the inlet, and therefore the flow is more stable up to higher rotational speeds.

Such a complexity of the flow in the back-sidewall gap results also in the shift of the map of the regimes. The three regimes were observed and the transitions between them were described as an alternative map for turbomachinery.

The throughflow does not change the state of the flow in the back-sidewall gap significantly in given rotational speeds and resulting flow rates. The throughflow is not strong enough to create neither the asymmetry of the flow field nor transform the existing flow structures. The destabilizing effect of the throughflow was observed only as a slightly earlier transition from regime III to IV.

Although the transitions between regimes I - III, III - IV and countless changes of flow character were achieved, no manifestation of those phenomena are distinguishable on the torque or axial thrust. The recorded data are smooth curves without abrupt changes.

The torque increases with increasing rotational speed, independently of the gap width, with no significant difference in the contours of wall shear stress among the geometrical configurations. Moreover, the presence of the throughflow (in the studied range) also does not make any difference in the torque.

Axial thrust also increases with increasing rotational speed, steeper compared to the torque. Its relation to the gap width is not so clear and more investigation would be necessary. The existence of the throughflow influences the axial thrust significantly. There is an observable qualitative difference in the pressure distribution between the closed cavity and the case with the throughflow, furthermore, the variation changes with the rotational speed. It results in lower, but the more complicated character of resulting axial thrust for different combinations of rotational speeds and flow rates as was discovered by the measurements.

Bibliography

[1] J. W. Daily and R. E. Nece, "Chamber dimension effects on induced flow and frictional resistance of enclosed rotating disks," *Journal of Basic Engineering*, vol. 82, no. 1, p. 217, 1960.

[2] B. Hu, D. Brillert, H. Dohmen, and F.-K. Benra, "Investigation on the flow in a rotor-stator cavity with centripetal through-flow," *International Journal of Turbomachinery, Propulsion and Power*, vol. 2, p. 18, oct 2017.

[3] B.-C. Will, *Theoretical, Numerical and Experimental Investigation of theFlow in Rotor-Stator Cavities with Application to a Centrifugal Pump*. PhD thesis, Universität Duisburg-Essen, 2011.

[4] M. M. de Beer, *Hydrodynamics and Heat Transfer of Single and Multiphase Flows in Rotor-Stator Spinning Disc Reactors*. PhD thesis, Department of Chemical Engineering and Chemistry, 2016.

[5] L. Schouveiler, P. L. Gal, and M. P. Chauve, "Instabilities of the flow between a rotating and a stationary disk," *Journal of Fluid Mechanics*, vol. 443, sep 2001.

[6] R. Hide, "On source-sink flows in a rotating fluid," *Journal of Fluid Mechanics*, vol. 32, pp. 737 – 764, 06 1968.

[7] J. Owen and J. Pincombe, "Velocity measurements inside a rotating cavity with a radial outflow of fluid," *Journal of Fluid Mechanics*, vol. 99, pp. 111 – 127, 07 1980.

[8] E. Crespo del Arco, P. Maubert , A. Randriamampianina , and P. Bontoux, "Spatio—temporal behaviour in a rotating annulus with a source—sink flow," *Journal of Fluid Mechanics*, vol. 328, pp. 271 – 296, 12 1996.

[9] E. Serre, S. Hugues, E. Crespo del Arco, A. Randriamampianina, and P. Bontoux, "Axisymmetric and three-dimensional instabilities in an ekman boundary layer flow," *International Journal of Heat and Fluid Flow*, vol. 22, pp. 82–93, 02 2001.

[10] J. W. Chew, "Prediction of flow in rotating DISC systems using the k-ϵ turbulence model," in *Volume 4: Heat Transfer; Electric Power*, ASME, jun 1984.

[11] J. W. Chew and C. M. Vaughan, "Numerical predictions for the flow induced by an enclosed rotating disc," in *Volume 1: Turbomachinery*, ASME, jun 1988.

[12] S. Poncet, M.-P. Chauve, and R.Schiestel, "Batchelor versus stewartson flow structures in a rotor-stator cavity with throughflow," *Physics of Fluids*, vol. 17, p. 075110, jul 2005.

[13] S. Poncet, R. D. Soghe, and B. Facchini, "Rans modeling of flow in rotating cavity system," in *V European Conference on Computational Fluid Dynamics (ECCOMAS CFD 2010)*, (Lisbonne, Portugal), June 2010.

[14] D. C. Wilcox, "Formulation of the k-w turbulence model revisited," *AIAA Journal*, vol. 46, pp. 2823–2838, nov 2008.

[15] F. R. Menter, "Two-equation eddy-viscosity turbulence models for engineering applications," *AIAA Journal*, vol. 32, pp. 1598–1605, aug 1994.

[16] E. Serre, E. C. D. Arco, and P. Bontoux, "Annular and spiral patterns in flows between rotating and stationary discs," *Journal of Fluid Mechanics*, vol. 434, may 2001.

[17] E. Tuliska-Sznitko, E. Serre, and P. Bontoux, "On the nature of the boundary layers instabilities in a flow between a rotating and a stationary disc," *Comptes Rendus Mécanique*, vol. 330, pp. 91–99, jan 2002.

[18] W. Lo, C. W. Chen, and C.-A. Lin, "Large eddy simulation of enclosed rotor-stator flow," in *TSFP DIGITAL LIBRARY ONLINE*, Begel House Inc., 2003.

[19] R. Pasquetti, E. Séverac, E. Serre, P. Bontoux, and M. Schäfer, "From stratified wakes to rotor–stator flows by an SVV–LES method," *Theoretical and Computational Fluid Dynamics*, vol. 22, pp. 261–273, nov 2007.

[20] J. Guelich, "Disk friction losses of closed turbomachine impellers," *Forschung im Ingenieurwesen*, vol. 68, 12 2003.

[21] C. Trivedi, M. Cervantes, and O. Dahlhaug, "Experimental and numerical studies of a high-head francis turbine: A review of the francis-99 test case," *Energies*, vol. 9, p. 74, 01 2016.

[22] R. E. Nece and J. W. Daily, "Roughness Effects on Frictional Resistance of Enclosed Rotating Disks," *Journal of Basic Engineering*, vol. 82, pp. 553–560, 09 1960.

[23] A. Poullikkas, "Surface roughness effects on induced flow and frictional resistance of enclosed rotating disks," *Journal of Fluids Engineering*, vol. 117, 09 1995.

[24] J. Daily, V. Asbedian, and W. Ernst, *Enclosed Rotating Disks with Superposed Throughflow: Mean Steady and Periodic Unsteady Characteristics of the Induced Flow.* Hydrodynamics Laboratory, Department of Civil Engineering, Massachusetts Institute of Technology, 1964.

[25] J. M. Owen, "An Approximate Solution for the Flow Between a Rotating and a Stationary Disk," *Journal of Turbomachinery*, vol. 111, pp. 323–332, 07 1989.

[26] B. Hu, D. Brillert, H. Dohmen, and F.-K. Benra, "Investigation on thrust and moment coefficients of a centrifugal turbomachine," *International Journal of Turbomachinery, Propulsion and Power*, vol. 3, p. 9, 04 2018.

[27] M. Daqiqshirazi, R. Torabi, A. Riasi, and A. Nourbakhsh, "Impeller gap width effect on losses in a water pump; numerical study," in *The 23rd Annual International Conference on Mechanical Engineering-ISME2015*, 05 2015.

[28] J. Gülich, *Centrifugal Pumps.* Springer Berlin Heidelberg, 2014.

[29] M. Gančo, "Axiálna sila hydrodynamických čerpadiel s radiálnym obežným kolesom." Slovenská technická unoverzita v Bratislavě - Strojnická fakulta, 1999. Habilitační práce.

[30] T. T. J. Kurokawa, "Study on axial thrust of radial flow turbomachinery," in *The Second International JSME Symposium-Fluid Machinery and Fluidics*, 1972.

[31] S. S. Evgen'ev, G. G. Petrosyan, and V. A. Futin, "Calculation of axial gasodynamic forces, disk friction losses and overflow in semiopen impellers of centrifugal compressors," *Russian Aeronautics (Iz VUZ)*, vol. 52, pp. 319–326, sep 2009.

[32] R. Klas, *Hydraulický návrh hydrodynamického stroje s vloženými lopatkami.* PhD thesis, Brno University of Technology, 2009.

[33] W. Li, "Model of flow in the side chambers of an industrial centrifugal pump for delivering viscous oil," *Journal of Fluids Engineering*, vol. 135, p. 051201, 05 2013.

Author's CV

Education

2017 - present	Brno University of Technology, Faculty of Mechanical Engineering, Energy Institute, Ph.D. programme: **Machines and equipment** (Disc friction loss in centrifugal pumps and hydraulic turbines)
2016 - 2017	Brno University of Technology, Faculty of Mechanical Engineering, Institute of Machine and Industrial Design, Ph.D. programme: **Machines and equipment** (Prediction of wear of hip replacements)
2014 - 2016	Brno University of Technology, Faculty of Mechanical Engineering, Institute of Machine and Industrial Design, master's programme: **Mechanical engineering design**
2011 - 2014	Brno University of Technology, Faculty of Mechanical Engineering, bachelor's programme: **Mechanical engineering**

Teaching activities

Hydromechanics Computational Fluid Dynamics Finite Element Method – ANSYS Classic Finite Element Method – ANSYS Workbech Machine Design - Machine Elements Machine Design - Mechanical Drives	Teaching excercises, laboratory practicum and computer-assisted excercises

Internships

2/2020 - 3/2020	Norwegian University of Science and Technology, Department of Energy and Process Engineering, Waterpower Laboratory

Work experience

8/2021 - present	Garrett Motion Czech Republic s.r.o., Tuřanka 100, 627 00 Slatina: **Development engineer**
3/2020 - 7/2021	Centrum Hydraulického Výzkumu spol. s r.o., Jana Sigmunda 313, 783 49 Lutín: **Senior researcher**
7/2017 - 1/2020	IMI Critical Engineering, K Letišti 1804, 627 00 Šlapanice: **FEM/CFD specialist**
2014 - 2016	Honeywell Technology Solutions, Tuřanka 100, 627 00 Slatina: **Simulation engineer**

Abstract

The thesis deals with an experimental and numerical study of the flow in sidewall gaps of hydraulic machines with a focus on low specific speed pumps. Although the fluid which fills the sidewall gaps represents only a very small portion of the whole volume of the machine, it can have a great impact on the flow in the whole domain. It can significantly influence the behavior, characteristics, and overall performance, especially in the case of low specific speed machines since it determines disk friction. The flow field in sidewall gaps also influences the pressure distribution inside a machine and thus generates axial thrust. The understanding of the flow in these regions is limited since it is based on the theory obtained for simplified geometry and its application in turbomachinery is questionable. In order to investigate the flow in the sidewall gaps of centrifugal pumps, a test rig including a real impeller has been designed and built up. It enabled observation of the flow in the backside wall gap for various operational regimes including optical measurement of velocity profiles, measurement of axial thrust, and frictional torque. A method for precise numerical simulation of such type of flow was developed to help reveal phenomena, which are not observable in the experimental apparatus and to extend the research to a wider range of operating conditions.

Dizertační práce je zaměřena na výzkum proudění v mezidiskových spárách hydraulických strojů s důrazem na čerpadla s nízkými specifickými otáčkami. Navzdory tomu, že tekutina v mezidiskových prostorách čerpadel zaujímá velmi malý objem, může výrazně ovlivnit proudění v celém stroji. To má následně vliv na provoz, charakteristiky a celkovou účinnost, zvlášť v případě čerpadel s nízkými specifickými otáčkami, protože stav proudění určuje vznikající diskové ztráty. Rovněž ovlivňuje rozložení tlaku a tím výslednou axiální sílu. Porozumění proudění v mezidiskových spárách je zatím omezené, současné poznatky vychází z teorie odvozené pro značně zjednodušený případ disku rotujícího v hladké válcové spáře. Použitelnost pro popis proudění ve skutečných hydraulických strojích je diskutabilní. Za účelem výzkumu proudění v reálném odstředivém čerpadle bylo navrženo a sestaveno experimentální zařízení umožňující pozorování proudění v zadní mezidiskové spáře pomocí optických metod, měření krouticího momentu a vznikající axiální síly. Také byla popsána metodika pro numerické simulace tohoto druhu proudění umožňující podchytit nestability a vírové struktury. Numerické simulace vhodně doplňují experimentální měření, rozšiřují rozmezí studovaných provozních podmínek a pomáhají popsat jevy, které by šlo měřením jen obtížně odhalit.